2 LOW-ENERGY ELECTRONS: MICROSCOPY AND SPECTROSCOPY

2.1 Introduction

The work in this thesis is built on three electron microscopy techniques, namely low energy electron microscopy (LEEM), electron-volt transmission electron microscopy (eV-TEM) and photoemission electron microscopy (PEEM). In contrast to other types of electron microscopy, these three techniques are based on low-energy electrons with energies in the 0-50 eV range. When low-energy electrons are incident on a sample, their interaction with the sample reveals information about the electronic band structure of the sample as outlined in Chapter 1. As the mean free path (MFP) of low-energy electrons is short, they are most sensitive to the surface. In the case of low-energy electron transmission microscopy (eV-TEM), the electrons traverse the full thickness of the sample, but the sample can only be a few atoms thick as low-energy electrons do not penetrate bulk samples to a measurable amount. In photoemission microscopy (PEEM), electrons from an occupied band are excited to the vacuum by illumination with ultraviolet (UV) light, also yielding low-energy electrons.

Electron microscopy means mapping the electronic properties of a sample with spatial resolution. In comparison to optical microscopy, an electron microscope is not limited by the wavelength of light, but by the de Broglie wavelength of the electron, thus LEEM reaches a resolution of 1.4 nm [1]. Still, the construction of the electron microscope can be understood from the analogy to optical microscopes, with electric and magnetic fields taking the place of mirrors and lenses [2,3]. The discovery of this analogy started the field of electron-optics and paved the way for building electron microscopes [4,5]. Like in an optical microscope, the electron microscope is constructed to have intermediate planes that form an image, referred to as the image plane, and back focal planes, referred to as the diffraction- or momentum plane in electron optics. Unlike in optics, the electron lenses can be adjusted in focal length or switched off by changing the voltage/current. This way the operator can change the magnification or switch between real-space and momentum space.

2.2 The ESCHER setup

The electron sources and contrast mechanisms in the different methods employed (LEEM, eV-TEM, PEEM) in this thesis are various but share one feature: In all cases, the collected electrons have a small, well-defined energy in the order of 0-50 eV. This enables the use of the same electron-optics in all three techniques for imaging, filtering, and projecting the electrons, to form an image of the sample. Figure 2.1a shows the sketch of such an instrument, the ESCHER aberration-corrected Low-energy Electron Microscope used for the work in this thesis. The sketch shows the different imaging techniques used and the different electron sources for LEEM (black), eV-TEM (green), and PEEM (violet arrow, UV light). The path of the electrons after leaving the sample (shown in red) is the same for the different techniques. The whole setup is under ultra-high vacuum (UHV), with the lowest pressure below 10^{-9} mbar in the sample chamber to avoid contamination of the sample surface.

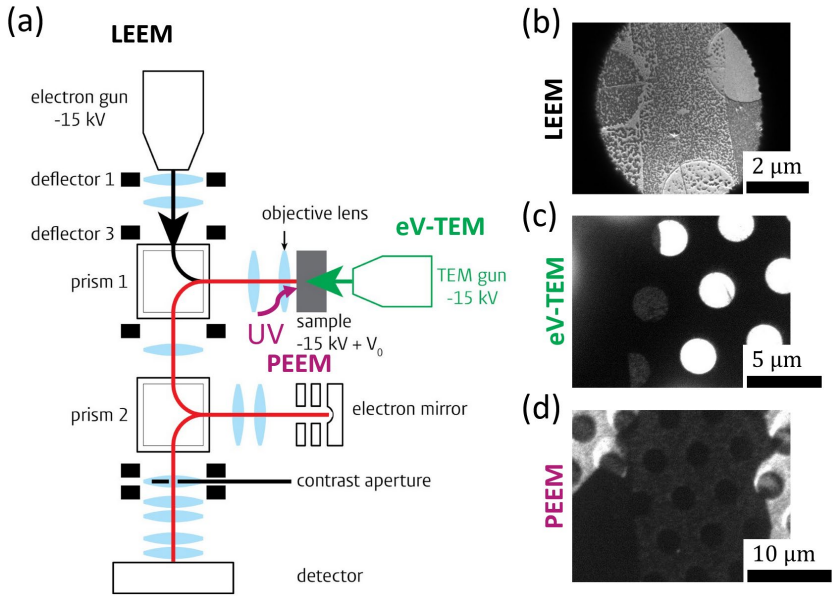

Figure 2.1: Different electron microscopy techniques in the ESCHER low energy electron microscopy setup. (a) Simplified sketch of the setup geometry with the electron sources in LEEM (black), eV-TEM (green) and the UV light for PEEM (violet). After interacting with the sample, all electrons take the same path (red) to the detector. Images of the same MoS_2 flake on a TEM grid recorded with LEEM (b), eV-TEM (c), and PEEM (d).

2.3 Low-energy Electron Microscopy (LEEM)

Foremost, the ESCHER setup was built as a Low-energy Electron Microscope aiming for improved real-space resolution. In LEEM mode, the electrons are emitted from a field emission gun at a potential of -15 kV at the top of the instrument (black in Figure 2.1a). The path of the electron is adjusted by deflector 1 (mostly in-plane momentum) and deflector 3 (mostly real-space position). The electrons are then directed toward the sample by the Lorentz force generated by a magnetic field that is oriented out of the plane of the sketch. This element, called the (magnetic) prism, is necessary to split the incoming and reflected electron beam.

The electrons travel through the objective lens, which is an electromagnetic lens. Between the objective lens kept at ground potential and the sample kept at $-15\ \mathrm{kV} + V_0$ the electrons are decelerated to an energy of $E_0 = V_0 \cdot e$, with the energy tunable through the voltage V_0. We remind ourselves that electric fields are conservative, thus the energy of the electron when interacting with the sample is only determined by the potential difference between the initial gun potential and the sample potential. As explained in Chapter 1, the electrons interact with the sample and are partially reflected, yielding the contrast in LEEM. The contrast strongly depends on the electron energy.

By convention, the energy reference $E_0 = 0$ eV is set to the point where the electrons just hit the sample, called the mirror mode transition. Thus, at $E_0 = 0$ eV the vacuum levels of the electron gun and the sample are aligned (whereas setting the same voltages would align the Fermi levels). The excitation of the objective lens is used to focus the electrons.

At LEEM low energies of 0-50 eV the reflection is dominated by elastically backscattered electrons, as inelastic processes, e.g., excitations of phonons and plasmons, only increase with increasing energy. When imaging in momentum space, we see these backscattered electrons as the specular spot. The first-order diffraction spots, that reveal the (inverse) lattice structure of a crystalline material, are visible at higher energies (typically > 25 eV), when the electron energy is sufficient to be converted to an in-plane momentum that matches the Bragg condition.

We note that, unlike in a scanning transmission electron microscope (STEM) or a scanning electron microscope (SEM), the electron beam (seen as the bright area in Figure 2.1b) hits an area of about 7 µm diameter of the sample all at once, like the in-line illumination in an optical wide-field microscope as opposed to a confocal microscope. The image is later created by projecting the reflected part of this beam on a two-dimensional screen. This enables imaging in real-time without scanning the electron beam.

After reflection, the electrons are accelerated by the electric field between the sample and the objective lens and travel through the magnetic prism. As the electrons now travel in the opposite direction, the Lorentz force directs them to the bottom, where the electrostatic transfer lens is situated. As the name prism suggests, the magnetic field also disperses the electrons of different energies, providing a means to resolve and filter electron energies.

The second prism and the electrostatic mirror are specific to the aberration-corrected LEEM setup. While other LEEM setups do without this part, it improves the resolution by correcting spherical aberrations to third order and chromatic aberrations to second rank. The voltages on the three mirror plates are tuned alongside the sample voltage for best correction at V_0. The electrons reflect from the 15 keV equipotential line without ever physically hitting the metal mirror plates. Again, the reflected electrons travel through the second prism and are deflected to the bottom.

The contrast aperture (below the second prism, see Fig. 2.1a) is placed in a diffraction-plane of the instrument to allow for filtering by placing an aperture in the beam path. The contrast aperture is placed around the specular spot (bright field) while looking at the sample in momentum-space. Then one can switch to the real-space image created with only the electrons that passed the contrast aperture, i.e., the electrons filtered in momentum space. The following four lenses, forming the projector column, are used to switch between real- and momentum-space and to magnify the image before the electrons hit the detector. The detector consists of a channel plate with variable gain and a fluorescent screen, that lights up when hit by electrons. The optical image on the fluorescent screen is then filmed with a CCD camera.

To record a LEEM IV (intensity as a function of voltage) spectrum, the electron energy E_0 is varied (typically in steps of 0.1 eV), and an image is recorded at every energy. As the intensity of a spectrum can vary over multiple orders of magnitude, the gain of the channel plate is automatically adjusted for adequate exposure. From this stack of images, the spectra of different sample areas are extracted and normalized by the calibrated channel plate gain curve [6]. We also record images at an energy where all electrons are reflected before reaching the sample (mirror mode, $E_0 < 0$) to normalize the reflection spectrum to the incident electron flux.

2.4 Electron Volt-Transmission Electron Microscopy (eV-TEM)

In eV-TEM, the electrons are emitted from a second electron gun added on the other side of the sample [7]. The electrons reach the sample at a tunable energy E_0, are partially transmitted, and then take the same path as the LEEM electrons would after reflection. Switching either the LEEM electron gun or the eV-TEM gun on, allows for consecutive imaging of the same sample area with both techniques, as both techniques use the same electron optical path for imaging the reflected and transmitted electrons, respectively. We will use eV-TEM in conjunction with LEEM to extract the elastic and inelastic MFP and identify states in the band structure. The LEEM image of a MoS_2 flake and the same area imaged in eV-TEM are shown in Figures 2.1b and c. The transmission spectra can be normalized to the flux passing an uncovered hole in the TEM grid at high energy.

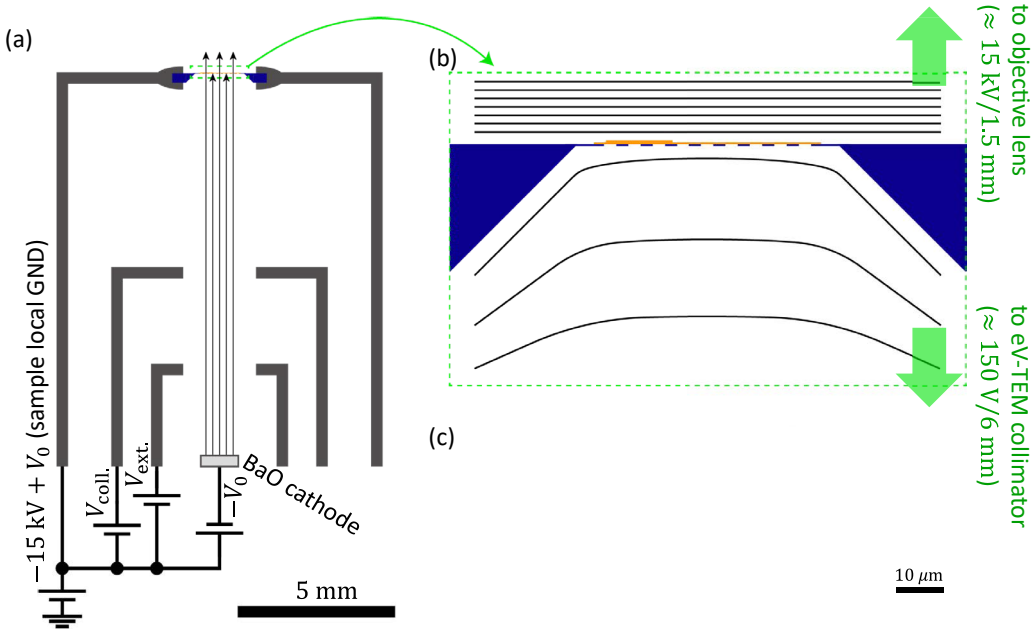

Figure 2.2: Geometry and electrical setup of the eV-TEM electron gun. (a) shows a cut through the cylindrically symmetric apertures used to guide the electrons emitted from a heated barium oxide (BaO) cathode to the sample. The equipotential lines (black lines in b) are curved close to the sample on a TEM grid, placed on top of the eV-TEM gun. The samples for eV-TEM are prepared on a silicon nitride TEM grid with a grid of holes (2.5 μm diameter) shown in c (purchased from Ted Pella, who also provided the SEM images in c).

The eV-TEM gun, which is integrated into the sample holder, is shown in more detail in Figure 2.2 together with its electrical setup. Figure 2.2a shows a cut through the electron gun, which is cylindrically symmetric around the electron beam axis. The electron gun consists of a barium oxide emitter, two apertures that act as electrostatic lenses, and the sample that is clamped onto the top. The eV-TEM gun is designed to fit in a modified sample holder [8], thus constrained to a diameter of about 1 cm and the use of 5 high-voltage electrical connections. The electron emitter is a barium oxide cathode (BaO, Kimball Physics), that thermally emits electrons when a current is passed through it and an extraction voltage $V_{\text{ext.}} \approx 50$ eV is applied. The barium oxide emitter is kept at a voltage of $-15\ \text{kV} - \Phi_{\text{BaO}}/e$ (the voltage equivalent to the work

function of BaO Φ_{BaO}), such that the electrons travel through the prisms at 15 keV like the electrons in LEEM mode.

After passing the extractor, the electron beam is collimated (i.e., reshaped to hit the sample as perpendicularly as possible) by the collimation voltage of $V_{\text{coll.}} \approx 150$ eV and finally reaches the sample at an energy of $e \cdot V_0$ with the sample voltage tuned to $V_{\text{sample}} = -15\ \text{kV} + V_0$. The electrons transmitted through the sample are then accelerated to the objective lens and enter the imaging electron-optics just like the LEEM electrons after reflection. In eV-TEM mode, the electron bundle illuminates the whole sample, such that large overview images can be recorded in real-time.

The power supplies that provide the voltages $-V_0$, $V_{\text{ext.}}$ and $V_{\text{coll.}}$ and the heating current supply for the BaO cathode are referenced to the sample voltage $V_{\text{sample}} = -15\ \text{kV} + V_0$ as shown in the circuit diagram in Figure 2.2a. This way the operation in LEEM mode remains unaffected when the eV-TEM gun is turned off and no additional high-voltage power supplies are needed for eV-TEM. In eV-TEM mode, one has to take care that both the sample voltage and the cathode voltage are adjusted in parallel, to keep the absolute potential of the BaO cathode – thus the energy of the eV-TEM in the prism – constant. The eV-TEM gun is turned off by setting the BaO cathode to a positive voltage, such that no eV-TEM electrons reach the sample, while keeping the cathode heated.

The eV-TEM samples, typically few-layer van der Waals materials, are prepared on a holey silicon nitride (Si_3N_4) TEM grid (PELCO®) purchased from Ted Pella. The TEM grid consists of a round carrier chip (3 mm diameter, 200 µm thick), that thins down to a 200 nm thin membrane (500 µm x 500 µm wide) in the center (see Fig. 2.2c) and has an array of holes (typically 2.5 µm diameter) patterned into the membrane. While the 80 nm Si_3N_4 membrane is transparent enough to high-energy TEM, it is not transparent for low-energy electrons. We coat the Si_3N_4 TEM grid in 5 nm platinum/palladium from both sides with a sputter coater (Cressington 208HR) to make it conductive. Then the layered materials are transferred onto the top, flat surface of the TEM grid.

The TEM grid with a layered sample is sketched in Figure 2.2b. As the TEM grid is surrounded by large electric fields, the sample itself must be considered part of the electron optics. The equipotential lines around the sample are sketched in Figure 2.2b. As the sample is usually oriented with the flat side – not the recessed side – towards the objective lens, the equipotential lines on that side are as flat as when imagining a typical sample in LEEM mode, e.g., a silicon chip with graphene on top. On the back side of the TEM grid, the equipotential lines follow the recessed shape of the TEM grid, obstructing imaging with electrons at perpendicular incidence at the edge of the recessed membrane. However, as the membrane is 500 µm wide and recessed with a 45-degree slope, and the electric field on the eV-TEM is comparably weak ($\approx 150\ \text{V}/6\ \text{mm}$ toward the collimator), the arising deflection of the electrons is weak on most of the grid. We will remark on the problems when flipping the TEM grid, thus putting the recessed side towards the objective lens where the voltage gradient is much stronger, in Chapter 4.

The energy resolution of the eV-TEM spectra is limited to ≈ 0.8 eV given by the energy spread of the thermally emitted electrons from the BaO cathode, while the cold field emitter of the

LEEM gun reaches an energy resolution of ≈ 0.3 eV. An improved electron gun, that uses a field emitter to reach the same energy resolution as in LEEM, was designed by Zhiyuan Cheng [9] as a M.Sc. student in our group but has not been produced yet.

2.5 Photoemission Electron Microscopy (PEEM) with polarized light

In photoemission electron microscopy ultraviolet light is shone on the sample and the electrons are emitted from the sample due to the photoelectric effect. The photon energy associated with the (deep) ultraviolet (UV) wavelength of the light must be sufficient to excite an electron from the highest occupied band to the (lowest band above the) vacuum level. The contrast is created by the different photoemissivity and work function in the material (and possible contamination). The electrons that overcome the work function barrier and leave the material are then accelerated toward the objective lens. As the photon energy used is typically just sufficient to reach the vacuum, the photoemitted electrons have a low energy of a few eV (and an even lower energy spread) and can thus be imaged by the same electron optics used for LEEM. The chirality induced spin selectivity effect is reported to manifests itself in a photoemission intensity depending on the polarization of the light (see Chapter 1). We add polarization control to PEEM to enable imaging this polarization-dependent contrast and thus spatially resolving the CISS effect.

Generally, the ESCHER setup is equipped with a mercury-vapor lamp filtered to emit a 254 nm wavelength (equivalent to 4.9 eV photon energy) for PEEM imaging [11]. While this photon energy is sufficient for photoemission from most materials, it may not be enough to overcome the work function of clean gold reported as 5.1 to 5.5 eV [12,13]. To reach this energy and match the setup used in previous photoemission experiments on chiral molecules, we installed a laser with 224 nm wavelength (equivalent to 5.5 eV photon energy). This deep UV (DUV) laser we use (PhotonSystems, HeAg70) is a pulsed laser. The pulse width is long (100 μs) and the power per pulse is low enough (14 μJ and 160 mW peak power) to not heat the sample or cause space charge effects. The maximum repetition rate is 20 Hz. The laser pulses are synchronized to the CCD camera trigger, such that every exposure contains exactly one pulse.

The use of a collimated laser beam also allows for control of the polarization, as needed for the photoemission experiments on chiral molecules with circularly polarized light, discussed in Chapter 6. The polarization control setup used to create circularly polarized light is shown in Figure 2.3, together with a schematic sketch of the optical components. The setup is clamped on the outside of the vacuum chamber of the ESCHER setup to a fused silica viewport facing the sample. The laser beam is aligned to the sample and the middle of the viewport with an adjustable mirror (DUV mirror, 190-600 nm enhanced aluminum coating, not in the photo Figure 2.3a).

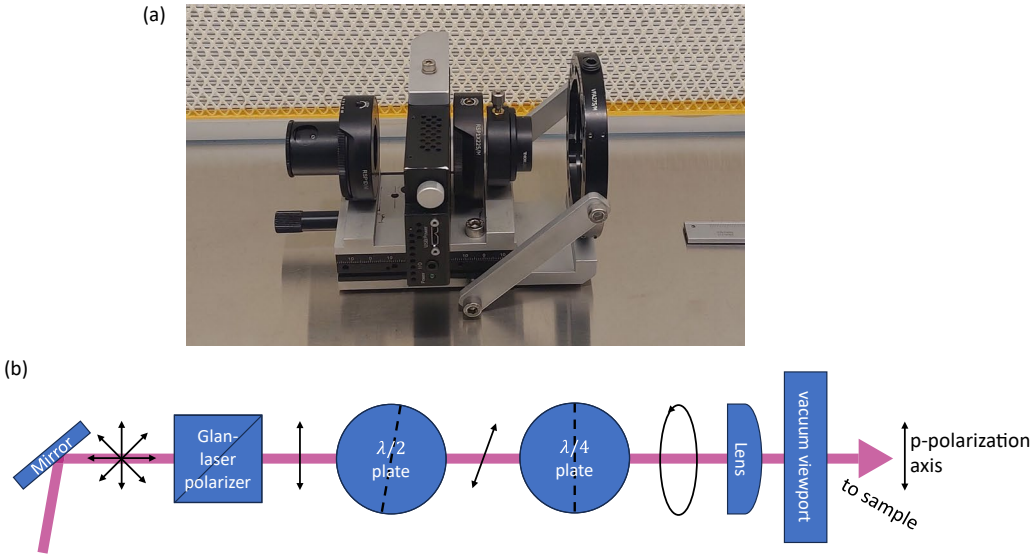

Figure 2.3: Polarization control setup for the polarization-dependent photoemission experiments. The polarizer, the motorized $\lambda/2$ plate, the $\lambda/4$ plate, and the lens are mounted on a bracket (photo a), that attaches to the sample vacuum chamber. The polarization of the light after each optical element is sketched with black arrows in b.

After reflecting from the mirror, the light passes the linear polarizer (a polarizing prism beam splitter, Glan Taylor prism). In the ESCHER setup, the laser beam is not perpendicularly incident on the sample, as the (electron-) objective lens is in that place. Therefore, two inequivalent linear polarization directions are defined relative to the plane spanned by the laser beam incident on the sample and its reflection, named p-polarization (that is parallel to that plane) and s-polarization (that is perpendicular to that plane). The polarizer is aligned to the s-polarization direction, where the absorption of light (and therefore the photoemission) is minimal. Then the linearly polarized light passes a $\lambda/2$ retardation plate, which changes the direction of the linear polarization. This $\lambda/2$ plate is mounted on a computer-controlled motorized stage. This setup has been used for experiments with linear polarized light of varying orientations.

For experiments with circularly polarized light, a $\lambda/4$ plate is added after the $\lambda/2$ plate. The fast axis of the $\lambda/4$ plate is aligned with the s-polarization direction, as the axes of the $\lambda/4$ plate define the short and long axis of elliptically polarized light, which should be symmetric with the s-polarization direction. Finally, a plano-convex lens (f=175 mm) is added, to focus the laser beam on the sample and thus increase the local light (and thus photoemission) intensity. While all the polarization control is mounted out-of-vacuum, the laser beam enters the vacuum through a fused silica viewport.

The typical experiment consists of acquiring images in one position of the motorized $\lambda/4$ plate, rotating the $\lambda/4$ plate to the angle mirrored along the s-polarization direction, and acquiring images again. As the intensity is low (shot noise and laser intensity pulse noise is the main source of error), this process is repeated 100 or 200 times. Then the difference between the images in each position gives insight into the (breaking of) symmetry.

References

[1] S.M. Schramm, Image Formation in LEEM and PEEM, in: PhD Thesis Imaging with Aberration-Corrected Low Energy Electron Microsc., Casimir PhD series, Leiden, NL, 2013. https://hdl.handle.net/1887/20843.

[2] H. Busch, Berechnung der Bahn von Kathodenstrahlen im axialsymmetrischen elektromagnetischen Felde, Ann. Phys. 386 (1926) 974–993. https://doi.org/10.1002/andp.19263862507.

[3] E. Brüche, H. Johannson, Elektronenoptik und Elektronenmikroskop, Naturwissenschaften 20 (1932) 353–358. https://doi.org/10.1007/BF01504926.

[4] M. Knoll, E. Ruska, Beitrag zur geometrischen Elektronenoptik. I, Ann. Phys. 404 (1932) 607–640. https://doi.org/10.1002/andp.19324040506.

[5] E. Bauer, Introduction: History, in: Surf. Microsc. with Low Energy Electrons, Springer New York, New York, NY, 2014: pp. 1–19. https://doi.org/10.1007/978-1-4939-0935-3_1.

[6] T.A. de Jong, D.N.L. Kok, A.J.H. van der Torren, H. Schopmans, R.M. Tromp, S.J. van der Molen, J. Jobst, Quantitative analysis of spectroscopic low energy electron microscopy data: High-dynamic range imaging, drift correction and cluster analysis, Ultramicroscopy 213 (2020) 112913. https://doi.org/10.1016/j.ultramic.2019.112913.

[7] D. Geelen, eV-TEM: Transmission Electron Microscopy with Few-eV Electrons, Doctoral dissertation, Leiden University, 2018. http://hdl.handle.net/1887/63484.

[8] D. Geelen, A. Thete, O. Schaff, A. Kaiser, S.J. van der Molen, R. Tromp, eV-TEM: Transmission electron microscopy in a low energy cathode lens instrument, Ultramicroscopy 159 (2015) 482–487. https://doi.org/10.1016/j.ultramic.2015.06.014.

[9] Z. Cheng, Designing a Novel eV-TEM Gun in COMSOL, 2022. https://hdl.handle.net/1887/3453471.

[10] R.M. Tromp, J.B. Hannon, A.W. Ellis, W. Wan, A. Berghaus, O. Schaff, A new aberration-corrected, energy-filtered LEEM/PEEM instrument. I. Principles and design, Ultramicroscopy 110 (2010) 852–861. https://doi.org/10.1016/j.ultramic.2010.03.005.

[11] R.M. Tromp, J.B. Hannon, W. Wan, A. Berghaus, O. Schaff, A new aberration-corrected, energy-filtered LEEM/PEEM instrument II. Operation and results, Ultramicroscopy 127 (2013) 25–39. https://doi.org/10.1016/j.ultramic.2012.07.016.

[12] W.M. Haynes, CRC Handbook of Chemistry and Physics, CRC Press, 2014. https://doi.org/10.1201/b17118.

[13] W.M.H. Sachtler, G.J.H. Dorgelo, A.A. Holscher, The work function of gold, Surf. Sci. 5 (1966) 221–229. https://doi.org/10.1016/0039-6028(66)90083-5.